Isotope Separator Upgrade Feasibility Study [ISU]

JW12-PM-EDT-ISU-01

"*Modelling the neutron and gamma fluences at KR2*"

N. Dzysiuk, S. Conroy, G. Ericsson

Division of Applied Nuclear Physics, Department of Physics and Astronomy,

Uppsala University, Sweden

Uppsala 2013

Content

I. Introduction
II. Neutral Particle Analyzer
III. Developing the MCNPX model
IV. Neutron spectra calculations
    i. DT scenario
    ii. DD scenario
    iii. DT and DD scenarios (after relocation)
V. Estimation of the KR2 background from neutrons and gammas
VI. Evaluation of the direct fast neutron component
VII. Conclusions
VIII. Data tables

I. Introduction and scientific motivation

Computer modelling is an effective approach to help in the evaluation of an instrumental upgrade. This work is devoted to modelling the neutron and gamma fluences at the JET low-energy Neutral Particle Analyzer (NPA) or in JET terms – "KR2". The work is done under Task Agreement **JW12-PM-EDT-ISU-01**.

Currently, the Joint European Torus is equipped with numerous diagnostics. One is the Neutral Particle Analyzer (Isotopes Separator). This diagnostic is designed to perform measurements of absolute fluxes of neutral particles emitted from the plasma. Besides providing absolute values it has the ability to distinguish the hydrogen isotopes and hence to study the isotopic composition of the plasma. The Isotope Separator Upgrade Feasibility Study (ISU) project is one part of the JET component of the EFDA 2012 Work Programme which includes 4 enhancement projects. Three of this set of diagnostic enhancements have been grouped into a package referred to as EDT (Enhancements for DT Operations).

The performance of the low energy NPA (KR2) is likely to be limited during the anticipated DT campaign in the present state of the diagnostic. The aim of ISU project is to plan for the necessary and needed work to obtain the best possible scientific results. The general planning involves essential maintenance and repair tasks as well as a plan for upgrading the detector and data acquisition system of the KR2. The plan for the hardware upgrade will be supported by modeling of the radiation fields at this diagnostic. According to the contract statements, the VR collaboration is involved to determine reasonable estimates of expected neutron fluxes at KR2 detector and electronics locations, to evaluate the need for relevant radiation hardness testing of detectors and electronics as well as to evaluate the potential need for improved radiation shielding if radiation fields interfere with measurement capabilities. The ISU project also aims to improve on the analysis of the KR2 data.

KR2 utilizes neutron and gamma sensitive detectors. Thus, in order to estimate signal to background in future DT campaigns, the neutron and gamma fluxes at the detectors must be known. Using the MCNPX code and a previously made model of JET fluxes are estimated for both DD and DT plasma. It has been suggested that KR2 may be relocated from its present location at Octant 3 to another port in Octant 8 in order to install a new Disruption Mitigation Valve (DMV). An initial study on the feasibility and impact of such relocation was carried out using the modeling described here. Based on these modeling results a decision could be taken if to perform lab tests to evaluate the tolerance of Si detectors and electronics to the expected radiation fields.

II. The nuclear particle analyzer operation principle

The NPA is designed specifically for measurements of the relative hydrogen isotope composition of Joint European Torus (JET) plasmas [1]. The neutral particles (atoms) are a result of recombinations inside the plasma (hot neutrals). Another contribution is impurities from the walls caused by radiation. The absolute fluxes of neutrals are connected to various important characteristics of the fusion reactions and a more accurate knowledge of their presence can thus be used for a better understanding of the state of the plasma.

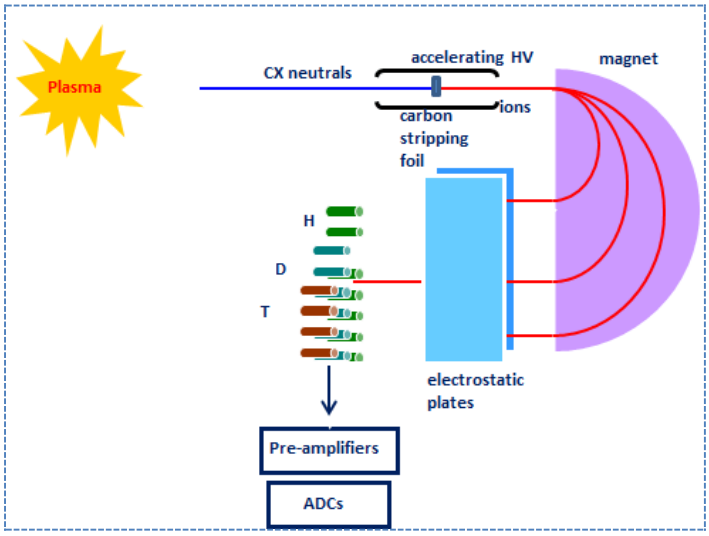

Fig.1 *The sketch of NPA*

Fig.1 gives a schematic representation of the KR2 working principle. It is based on charge exchange (CX) process whereby a hydrogen ion gains an electron from a background atom to get neutralized and thereby ceases to be confined by the magnetic field. The NPA measures the flux and energies of lost neutrals to deduce the ion energies, plasma temperature and the radial profile of the hydrogen isotope composition of the plasma. Neutral particles which are passing through the magnetic field in the direction of the KR2 can escape the plasma and reach the diagnostic. At the entrance of the diagnostic there is a thin carbon stripping foil for ionizing the neutral particles. In order to increase the total detection efficiency the ions pass through an accelerator voltage (100 kV) where the energy of the ions is increased. The separation of the ions by energy occurs in a vacuum chamber and consists of two sequential steps. First, by means of a magnetic field there is a separation in momentum (energy) dispersion since ions of different energies move along different radii. Second, the ions traverse an electrical field for mass separation. In the current version of the

diagnostic a set of three arrays of CsI scintillators are used for ion measurements. In this report, the use of silicon detectors is considered as a new type of detection system.

III. Developing the MCNPX model

The first stage of this work is the development of the computer model of the KR2 diagnostic. This task was accomplished with the MCNPX code based on the Monte Carlo approach [2]. MCNPX is a general code for calculating the time-dependent continuous-energy transport of neutrons. The code is well suited to simulate complicated particle transport because it uses continuous cross section data. It treats an arbitrary three-dimensional configuration of materials in geometric cells.

In order to reproduce the real features of this diagnostic the available information on geometry, materials, and constituents was used. The geometry information and physical dimensions of elements were taken from drawings and provided technical specifications. In the input file the elements of the NPA were defined utilizing the macrobodies (three-dimensional figures) and planes. The materials are defined by isotopes accordingly to material composition (air, stainless steel, lead, silicon, polyethylene, natural copper and iron). The information on the material densities was taken from the chemical element properties table. It should be stressed that MCNPX uses detailed point-wise cross section from evaluated nuclear data libraries to provide the most reliable simulations.

The considered detection system is placed inside a shielding to withstand the harsh conditions expected in DT and DD operations. The shielding consists of three main layers: an outer made of stainless steel (2 cm), followed by a layer of water expanded polyethylene WEP (18 cm) and a final layer of lead (7 cm). This layered structure can be seen in the 3D model (Fig.2, left panel).

The following geometrical elements have been included in the model: shielding (3 layers), the vacuum chamber which incorporates the body of the magnet and its excitation coils, electrode, elements of bottom, side, top and central support, two pump systems, coils, yoke, ion guide, detector unit, flanges, poles, side plates. They were modeled precisely because these massive elements are the most influential on the neutron scattering as well as a gamma background increasing. The full-scope KR2 model is shown in Fig. 2 where the diagnostic is presented with (left panel) and without (right panel) shielding, such that all elements and shield layers are clearly visible.

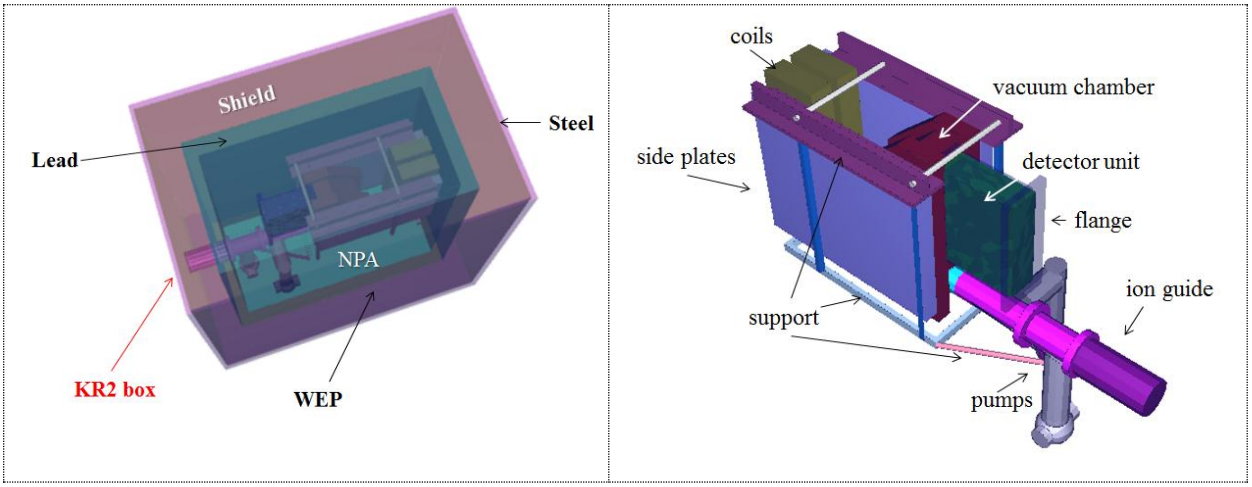

Fig.2 *The MCNPX 3D model of the KR2 diagnostic*

As mentioned above, besides having a complicated external shape the vacuum chamber also has an internal structure with magnet poles. In order to give accurate information the shape was reproduced in the same detail (see Fig. 3). In this plot, the Si detector is represented by a dark band inside the detector extension box which was made transparent to show the position of the silicon detectors.

Precise information on dimensions of the Si detectors was not available that at the time the model was built. We have assumed it was made of strips of Silicon placed on a backing substrate. It should be emphasized that the array of detectors is not a single layer but rather an array of several materials. The active silicon layer is of 5 μm thickness, then 250 μm of silicon substrate, then 25 μm of copper and 1 mm of FR4 (epoxy) material.

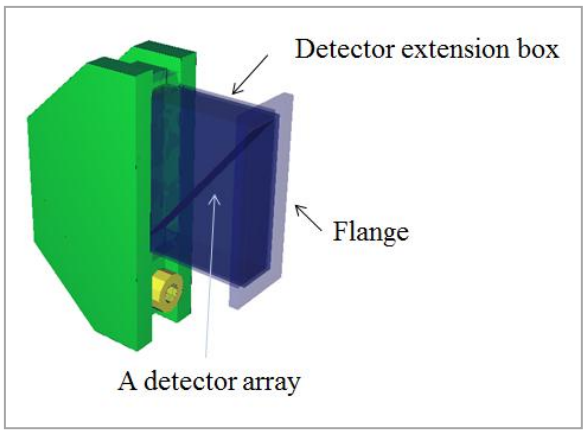

Fig.3 *External view of the MCNPX model of the vacuum chamber. In order to show the position of silicon detector plane (diagonal dark band) the detector extension box was made transparent. The Silicon detector is placed in vacuum.*

The physical dimension of the KR2 box is L × W × H = 187 × 116 × 184 (cm). The dimensions have been taken from the available drawings. Fig.4 shows a photo of KR2 in the JET Torus Hall (Octant3).

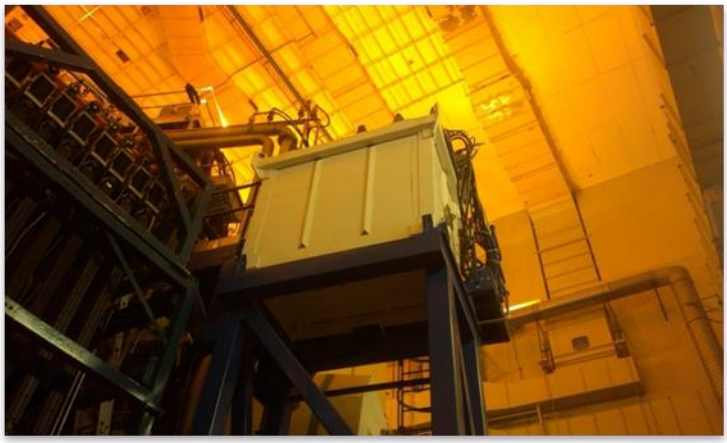

Fig.4. *The KR2 external view (photo)*

IV. Neutron spectra calculations

The plasma neutron source was calculated for a previously defined plasma profile using the TRANSP code. The source is isotropic in emission and anisotropic in spatial distribution. It is supposed to mimic a typical 3.5 MA H-mode plasma of 10 keV temperature.

There are two main fusion reactions which are widely used. The fuel for such reactions consists of the hydrogen (H) isotopes: deuterium (D) and tritium (T).

$$D+D \rightarrow {}^{3}He\ (0.82MeV) + n\ (2.45MeV)$$
$$D+T \rightarrow \alpha\ (3.54MeV) + n\ (14.03MeV)$$

The D-T reactions have a much larger cross-section than those for D-D, and so a D-T mixture offers an easier route to power production than pure deuterium. The first set of calculations was performed with a DT plasma source. However, since most of JET operations use a DD plasma source (> 99%), a similar set of calculations were performed using 2.5 MeV neutrons instead of 14 MeV. The calculations of neutron fluxes have been done using the model described above. In order to minimize CPU time the calculations were performed in two sequential steps.

1. The first stage of the calculations used the large JET model [3] with KR2 modelled crudely inside a box. In a long calculation (10 days) particles entering the box were stored for use in

the next step. That run was made on a computer claster of 96 nodes. The neutron spectrum was recorded on the surface of a box with dimensions: 250 × 250 × 120 cm. The detailed KR2 model was placed inside this box by means of the MCNPX spatial transformation card (TR) which allows to move any element in the space. Fig.5 shows the large JET model with a box included (orange) for recording the neutron spectrum for the next step. Any problems with the large model will propagate through all later models. Unfortunately, after this work was done the neutron calibration of JET has indicated that the Lower Hybrid part of the model may have been too strongly attenuating. That analysis is still ongoing at the time of this report.

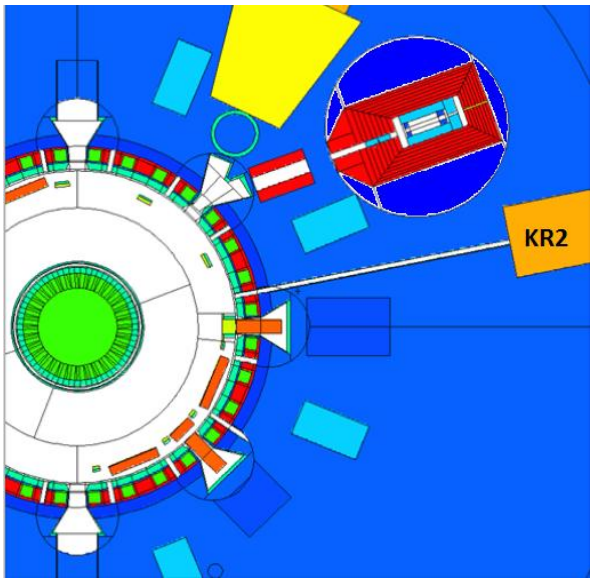

Fig.5 *Cross section through the large JET model*

2. The second step is a propagating the stored neutrons into the detailed model of the KR2. Trajectories of neutrons crossing a certain surface are stored in the first run. In the second run these trajectories are used to launch the neutrons in the NPA model. As the interaction points for each neutron are determined randomly, the same trajectories can be reused in the NPA model. This allows the NPA model to effectively simulate a much greater number of trajectories than in the first model. This is an approximation but when sufficient trajectories are stored and the main interest is to investigate bulk shielding problems it is a reasonably good one (runs effectively 100 times faster). Having the information on the vertical position of the KR2 port the modeled diagnostic was assumed aligned with the main line-of–sight.

i. DT scenario

In the first set of calculations the modelled diagnostic is located in Octant 3. The obtained results are presented in Fig.6. For analysis the average neutron fluxes were calculated over the volume of the different shield layers namely the external KR2 box, the lead layer, the polyethylene layer and "Interior" – the internal space (air) between the internal surface of the lead and the NPA itself. All data including uncertainties, are summarized in Table 2.

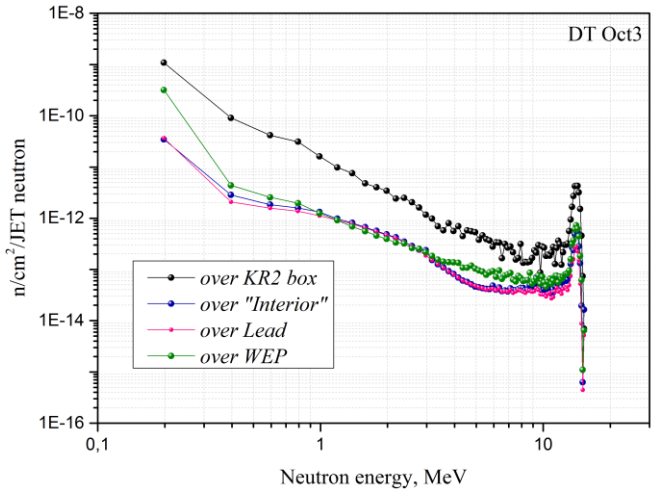

Fig. 6 *Calculated neutron spectra at the KR2 (Oct 3) for DT operations*

It could be seen from Fig.6 that neutron attenuation takes place when moving into the KR2 box. The shielding is sufficient to suppress the neutron flux by a factor of ~15. The 14 MeV flux incident on the detectors is reduced from $1.6 \cdot 10^{-11}$ to $1.0 \cdot 10^{-12}$ (n/cm^2 per JET neutron) (see Fig.6). The total fast neutron flux (>1 MeV) is reduced by a factor 8 from $7.2 \cdot 10^{-11}$ to $9.1 \cdot 10^{-12}$, and the attenuation improves further at lower energies.

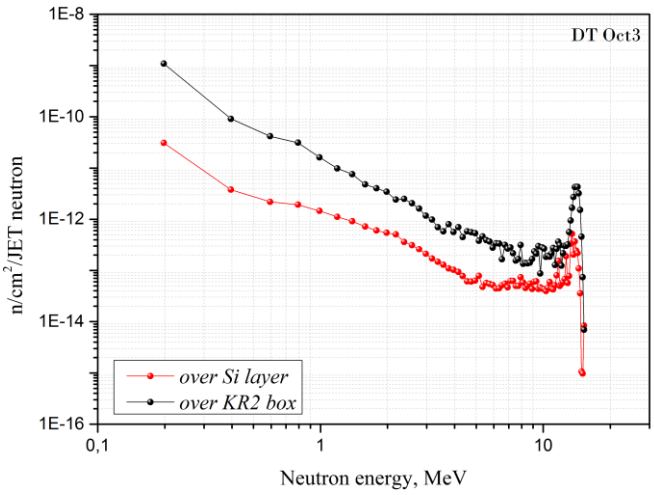

Fig.7 *Calculated neutron spectra at the KR2 (Oct 3) for DT operations*

In Fig.7 is shown a superposition of neutron fluxes calculated over the silicon layer and the external surface of the KR2 box. The units of the neutron flux are neutron per cm^2 per JET neutron. Multiplying the data given in Table 2 by the JET DT neutron rate gives the neutron flux per second in each zone.

Another key issue is the gamma background. Unfortunately the information on real gamma fluxes in the Torus Hall is not available. However, the gamma flux in the Torus Hall is anticipated to be lower than the neutron flux and the flux towards the KR2 detector position to be strongly attenuated by the lead layer. For the purposes of this analysis it is therefore presumed negligible at the Si layer. Gammas generated by neutron interactions in the shield can be modelled with MCNPX and the results are shown in Fig.8. A comparison is made between gamma fluxes calculated at a Silicon layer and the "Interior". The level of gamma flux at the Silicon is higher which indicates that surrounding materials (vacuum chamber, flanges) can generate extra gamma-rays.

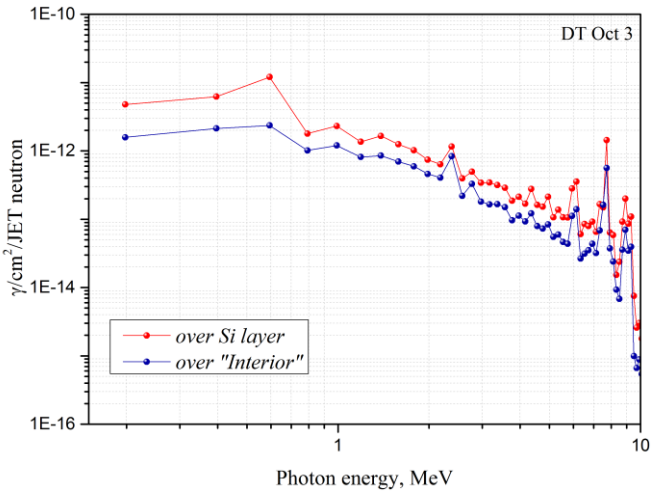

Fig. 8 *Gamma spectra in DT campaign (Octant 3)*

MCNPX allows the representation of the neutron field as a contour plot. It could be done with utilization of the TMESH tally [2] as an approach for graphical displaying neutron or gamma flux quantities. Results of displaying of the neutron and gamma fluxes for a region centered on KR2 are shown in Figs.9-11. This is a useful approach to check if for instance the modeled diagnostic is in the correct place and that the neutron source is generated properly. Particles are tracked through the independent mesh as part of the regular transport problem. The considered area of the model is divided into a number of small cells making a grid and the neutron flux is calculated in each cell. As can be seen in Fig.9 the value of neutron flux is proportional to the color scale.

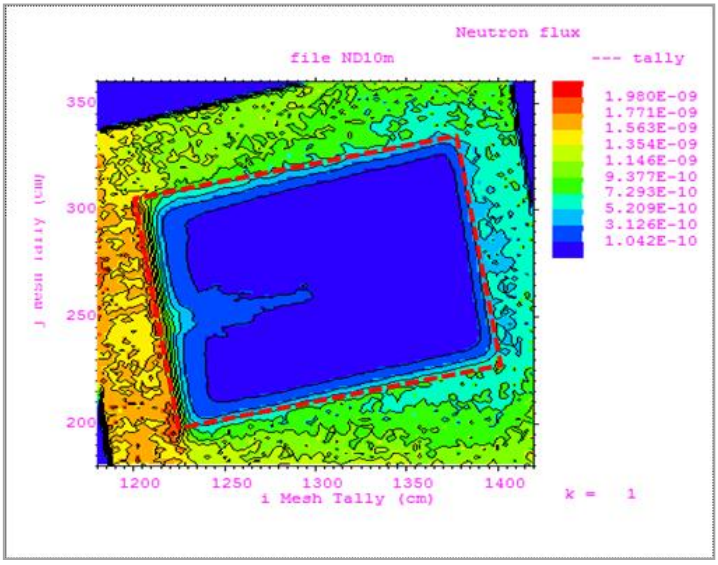

Fig.9 *Top view of KR2, neutron flux distribution.*

Also, such displaying is applicable to check for geometry errors. In Fig.9 there is a MESH grid done for the neutron field in the region of KR2. The KR2 box is indicated by red dashed line. The neutron field outside the shield appears nonuniform due to the limited number of neutrons recorded in the first stage calculation. At the shield, clearly the side facing the plasma receives a higher flux than the other sides. The effect of the shield can be seen in the decreasing flux levels further into the shield. The colour corresponds to the neutron flux with neutron/cm^2/JET neutron units.

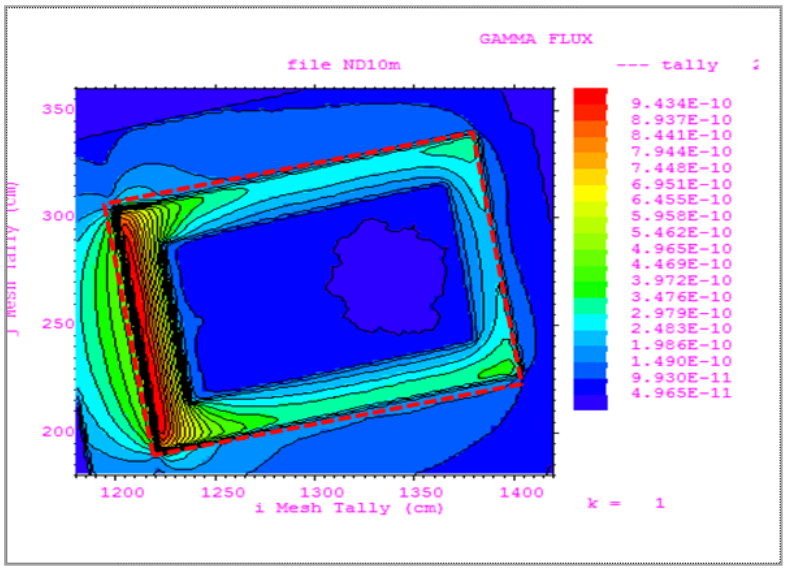

Fig. 10 *Top view of KR2, gamma flux distribution*

Fig.10 shows a contour plot for the gamma field distribution at the KR2. The external KR2 box is indicated by red dashed line. In comparison to Fig.9 this plot looks more smooth and uniform. It should be stressed that the gamma fluxes in the H mode at JET are not modelled due to lack of information on the composition of materials around the vessel. There is not a measured field which could be used and applied to the outside of the NPA. Here gammas are a result of neutron interactions with material. From the plot it is clearly seen that gamma generation is most intense from the outer surface of the KR2 shield box and decreases as we go deeper inside the shield. The generated gammas are propagating isotropically. Gammas produced in the shield are generally absorbed quickly. This leads to the gamma intensity being roughly proportional to the local neutron flux.

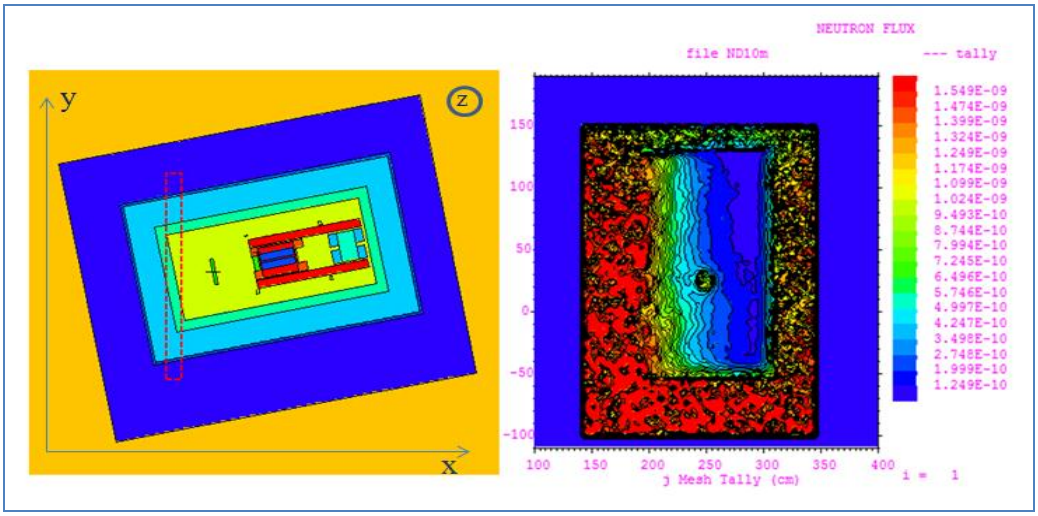

Fig. 11 *Neutron flux. A front view cut.*

Fig.11 displays a contour plot of the neutron flux calculated within a slice through the front facet of the KR2 box. Clearly, this front cut view is somewhat non-symmetric (see Fig.11). This is explained by the KR2 box being located at an angle with respect to the reference coordinate system but the mesh area could only be defined in the reference system. The right panel of Fig.11 shows the average neutron flux calculated in the dashed box region indicated at the left panel of this figure. In this slice the left side looks thicker and the observed gradient of color shows the shield layers. The area in red corresponds to higher neutron fluxes. It could be noticed that the bottom side (at (–50) – (–100) cm) is more exposed to neutrons because those are primarily scattered neutrons from the floor. The distance to the torus hall floor is three times shorter than to the ceiling.

ii. DD scenario

The NPA is going to be operated in both DD and DT campaigns and the evaluation of neutron fluxes in DD campaign is required as well. The main results of calculations of neutron and gamma spectra for DD operation are shown in Figs.12-13. These data including uncertainties are summarised in Table 3. The calculations have been performed in the same two-steps way as described above for the DT scenario.

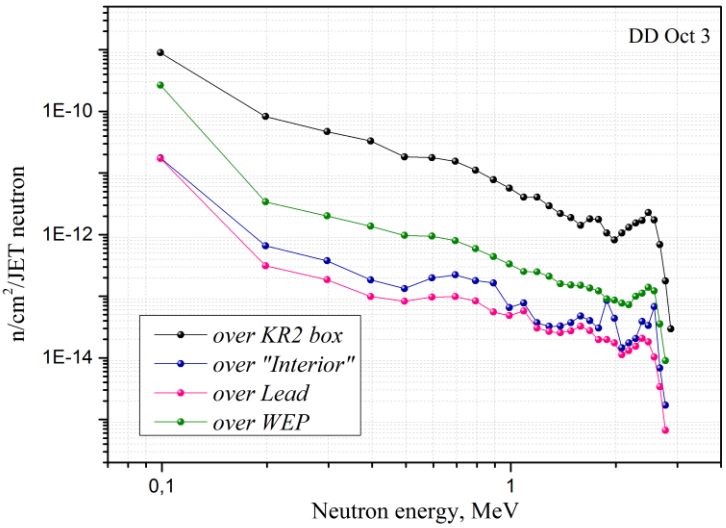

Fig. 12 *Calculated neutron spectra at the KR2 (Oct 3) for DD operations*

Fig. 12 shows the comparison between neutron fluxes calculated over different layers. The black curve corresponds to the neutron flux over the external KR2 box, the green curve - the WEP layer, the blue curve - "Interior" and pink one – the lead layer. By analysis of fluxes over the KR2 box and "Interior" we can conclude that for the DD scenario the neutron flux is suppressed more effectively since the shield is more efficient at lower neutron energies.

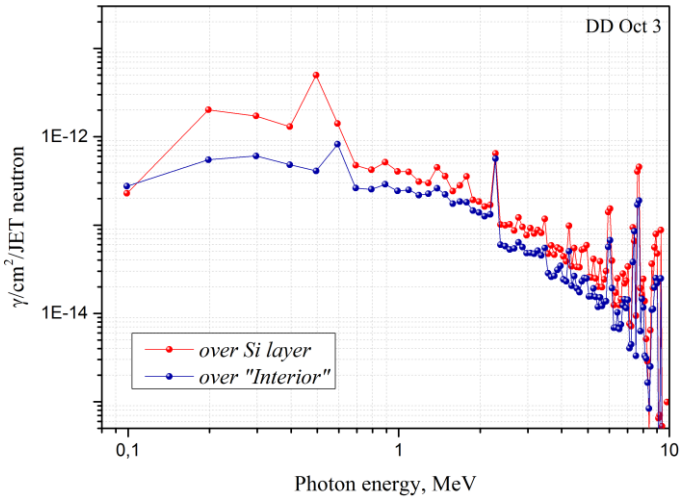

Fig. 13 *Gamma spectra in DD operation (Octant 3).*

In Fig.13 there is a comparison between the gamma spectra at the Si detector area and the internal space of KR2. The flux over the Si layer is higher due to the extra material surrounding the silicon detectors. The evaluation of gamma fluxes is important since they could induce a source of background in the detector's response.

iii. DT and DD scenarios (after relocation)

Currently KR2 is located in Octant 3 but it may be moved to Octant 8. Below is a cut through a full scale CAD model of the relevant section of the JET Hall. The KR2 box is indicated by a light green box.

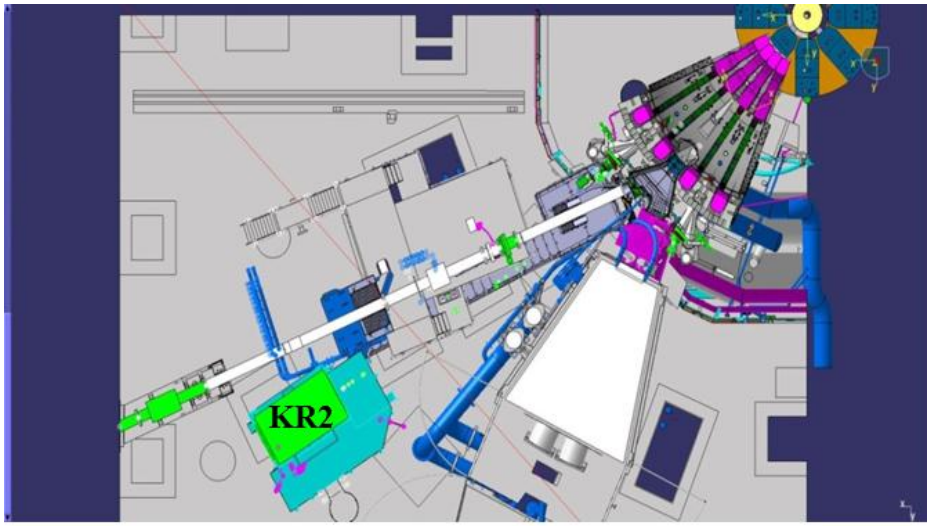

Fig. 14 *Sketch of KR2 location in Oct 8 of JET Torus Hall*

All neutron spectra calculations have been performed in a two-steps way described earlier. The first step is a preparation of neutron sources for the new KR2 position. For this purpose the neutron field was recorded onto a surface of the box placed in a given place in Octant 8. The results of the calculations for DT neutrons in the new position are presented in Fig.15.

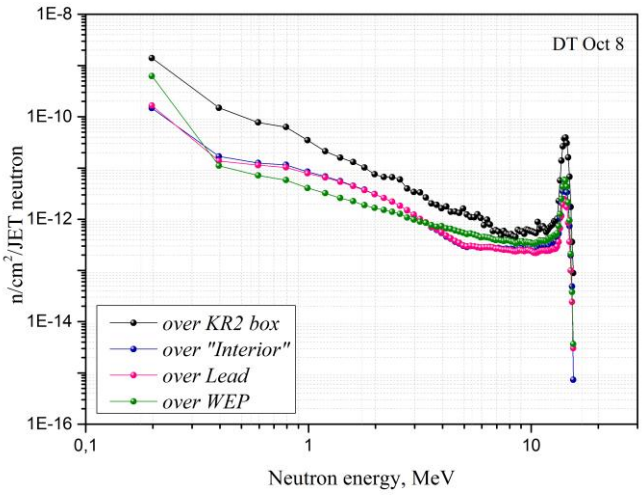

Fig. 15 *Calculated neutron spectra at the KR2 (Oct 8) for DT operations*

The spectra calculated for the DD neutrons are shown in Fig.16. The shield reduces the neutron flux by a factor 15-20. Note however, that the neutron flux is in general about one order of magnitude higher in Oct 8 compared to Oct 3, which makes it a less favourable for the diagnostic.

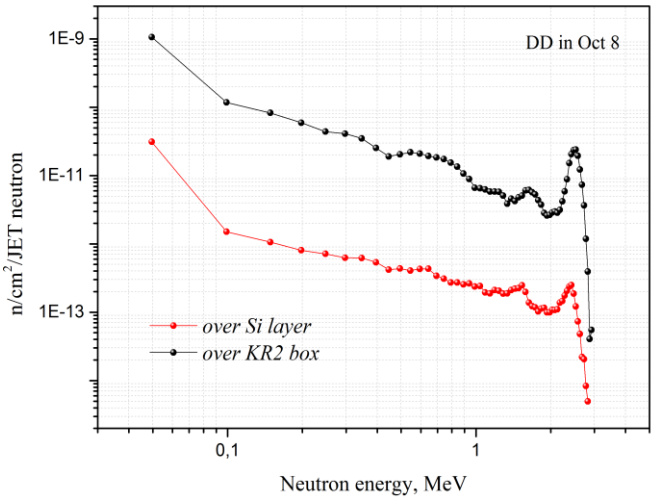

Fig. 16 *Calculated neutron spectra at the KR2 (Oct 8) for DD operations*

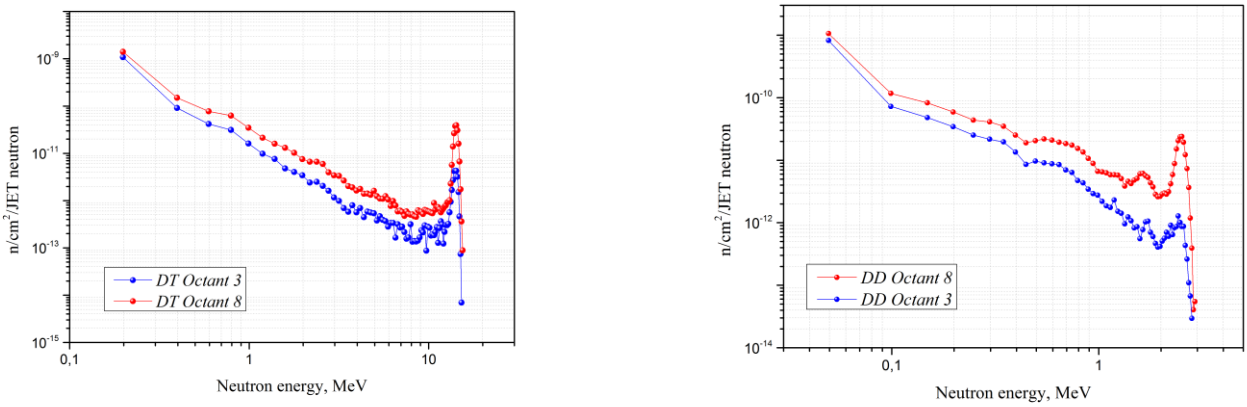

Fig. 17 *Comparison between DD and DT neutron fluxes simulated at active Si layer*

The comparison between calculated neutron fluxes at the Si layer for both DD and DT scenarios and locations is presented in Fig.17. Obviously the level of neutron flux in Octant 8 is higher which will cause more harsh conditions for Silicon detectors.

V. Estimation of the KR2 background from neutrons and gammas

In the NPA upgrade the silicon detectors are the main system to detect the hydrogen ions. Unfortunately when the NPA is operating the neutron and gamma fluxes cannot be reduced completely. The Silicon detectors are sensitive to such neutron and gamma-rays background and their efficiency is proportional to the volume. Thus the level of background registered in the Si detector primarily depends on the detector thickness and intensity of radiation field. Therefore, a modelling of the deposited energy distribution in the active Si detector layer is required in order to assess the signal to background situation.

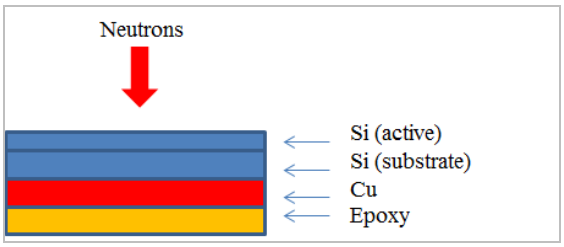

Fig.18 *The scheme of the layer structure*

The structure of the Silicon detector array is not simple since it is not a single layer (see Fig.18). The Si detectors are going to be coupled to a Si-Cu backing and support platform. This platform includes 250 μm of Si substrate followed by 35 μm of Cu and 1 mm of the epoxy material.

In the active silicon layer (n,α) and (n,p) reactions as well as elastic and Si(n,n')Si* inelastic scattering are the most probable processes. The ranges of alpha-particles and protons in pure Si were calculated with the SRIM code [4] for three typical energies (1, 5, 10 MeV) which we will have in the case of 14 MeV neutron interactions. The information on reaction thresholds and Q values is taken from the US National Nuclear Data Center [5]. The results are summarized in Table 1 below.

Table 1: *Top: Range of proton and α-particles in Si. Below: Reaction thresholds and Q values of (n,α) and (n,p)reactions in Si*

Range (μm) in Si (the SRIM code)			
	1 MeV	5 MeV	10 MeV
Protons (p)	20	230	750
Alphas (α)	4	27	75

Reaction	**Reaction threshold (MeV)**	**Q value (MeV)**
(n,α)	2.749	-2.653
(n,p)	3.999	-3.859

In order to see how the thickness of the active Si layer can influence the total energy deposition some additional calculations were performed. Neutrons generated by a point 14-MeV neutron source were propagated through the silicon layers of 5 μm, 25 μm, 100 μm, 1 mm, and 1 cm thickness. The results of these calculations are shown in Fig.19.

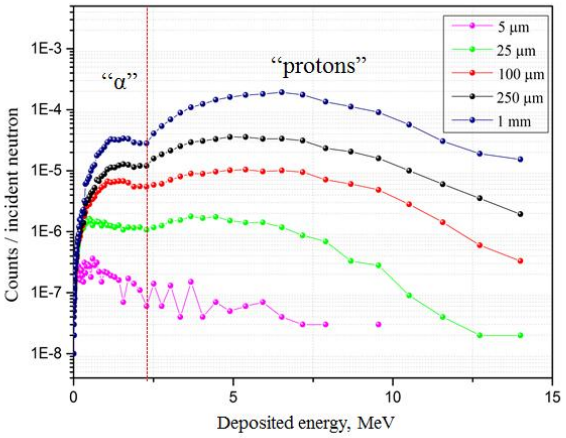

Fig. 19 *Distribution of deposited energy by proton and α-particles in Si active layer of different thickness (5, 25, 100, 250, 1000 μm)*

Fig 19 can be considered to have two regions. The first region is E_{dep} = 0 – 2 MeV which mainly caused by the alpha-particle energy deposition due to their short ranges, while the E_{dep} = 2 – 14 MeV resulting from the proton deposition.

Neutrons can deposit energy in a silicon layer by means of secondary particles produced in nuclear reaction in adjacent layers. Such deposition can be significant and thus make a contribution to the total count rate of the Si detectors. As was shown in Table 1 above, the range of the produced secondary particles are quite long that is why the neighboring layers will contribute to the total count rate of silicon detector. In order to study this issue additional calculations were performed. Using the initial calculated neutron flux over the silicon cell the average distribution of alpha-particles was simulated with the MCNPX code for three cases as presented in Fig.20. The blue curve corresponds to a case when all actual layers were present. The red curve represents the case when the Si substrate and copper layers were filled with vacuum. The black curve corresponds to calculation when the Si substrate was filled with vacuum.

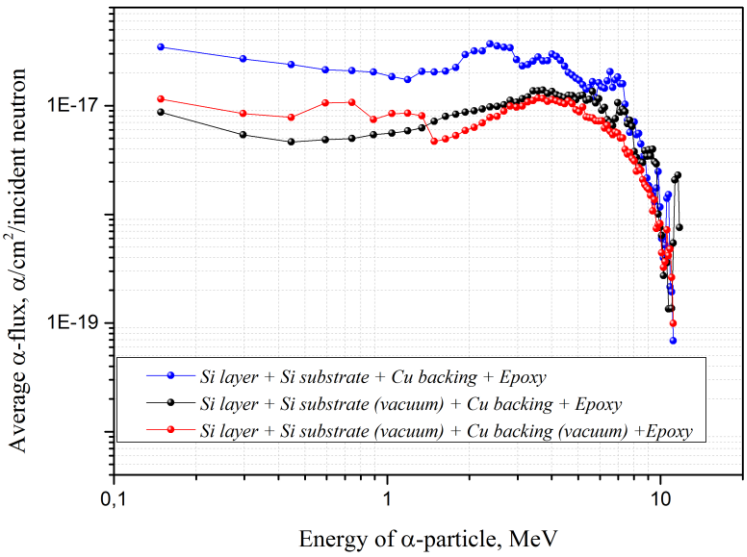

Fig. 20 *Comparison of the simulated α-distributions*

The ranges of expected alpha particles are quite small but still the alphas produced in neighbour layers can penetrate to the active silicon layer and make a contribution to the total count rate.

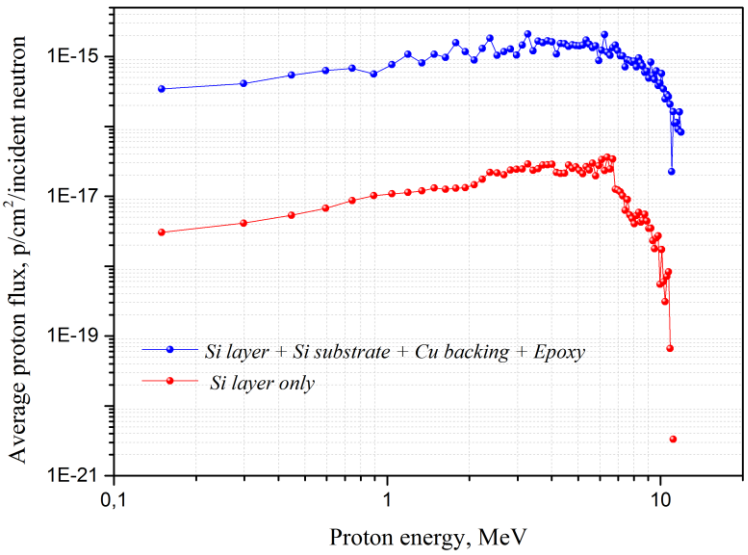

Fig. 21 *Comparison of the simulated proton distributions*

Fig.21 shows the comparison between average proton distributions calculated over the silicon layer for two cases. The blue curve corresponds to a situation when all layers are present. The red curve represents the result of calculation which was done for a case when the Si layer only was present and all the other layers were filled with vacuum. It is clearly seen that protons produced in neighbour layers can penetrate to the active silicon layer and give a significant contribution to the total counting rate.

1. The calculation of the total energy deposition is very relevant and needed but is, in the case of a very thin Si layer, problematic. The calculation of deposited energy due to the reactions is based on the energy deposited by the secondary proton and α-particles. MCNPX allows the calculation of them with some limitations. However, a direct calculation would take more time then was available in order to get an acceptable level of statistical accuracy.
2. One challenge in using MCNP is to minimize the computing expense needed to obtain a result with acceptable uncertainty. Variance reduction techniques are approaches to apply to reduce the computational effort for a particular problem and improve the efficiency of a calculation implemented in the code. Unfortunately in MCNPX the pulse-height deposition process is incompatible with the most applicable variance reduction methods.

3. Splitting the simulation into a series of calculations allows a reasonable estimate of the energy deposition to be produced in a manageable time frame. That is why all necessary calculations have been done in two steps.

The first step: the neutron spectrum (Fig.22, left), here for the KR2 location in Octant 3, was calculated as described above by means of the full MCNPX model.

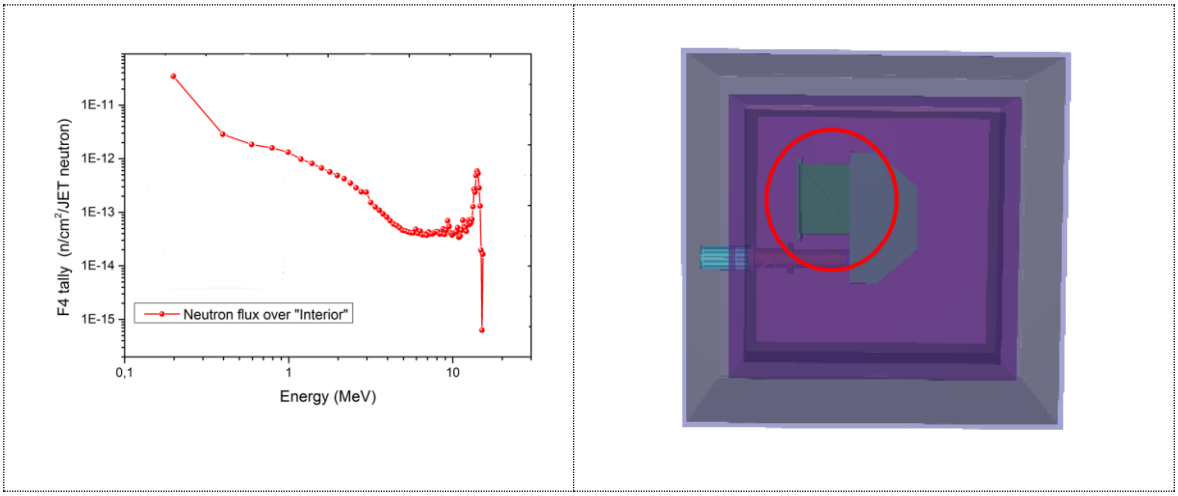

Fig. 22 *Neutron spectrum at "Interior" (left); Simplified model (right)*

Second step: neutrons of that spectrum were emitted isotropically from an imagined sphere of known radius. That was done with a simplified model (Fig.22, right panel). Calculations of the total energy deposition have been performed for the neutron and gamma spectra separately.

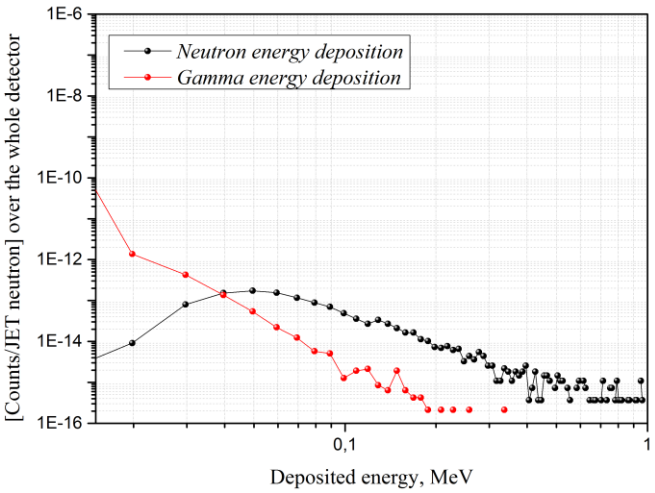

Fig. 23 *Total energy distribution in a 5 μm Silicon layer*

In such case it was possible to avoid a problem with the variance reduction utilization. The results of these calculations are presented in Fig. 23. The black curve describes the energy deposition in a Si detector caused by neutrons while the red curve represents gamma-rays. The calculations have been done for the 0 – 14 MeV energy deposited range with step of 20 keV for convenience of a future comparison to the experimental data. Unfortunately the range which starts from 100 keV has poor accuracy while the low energy range is better defined. This low energy region is very relevant because it is the working range of the NPA.

VI. Evaluation of the direct fast neutron component

KR2 is located quite far from the vessel but some amount of neutrons from the plasma are going to pass through the KR2 port (see Fig.24), avoiding the shield to reach the detector area. Unfortunately the number of stored events in the first run using the big JET model is not high enough for the small area of the KR2 port and we do not have sufficient events to model this area very well. That is why a second evaluation of the effect of fast neutrons coming through the KR2 port was done in two steps.

First step: A simplified geometry was used where the KR2 box is coupled to a collimator tube of 12 m length. A point source of 14 MeV neutrons was placed in front of the collimator (Fig.24).

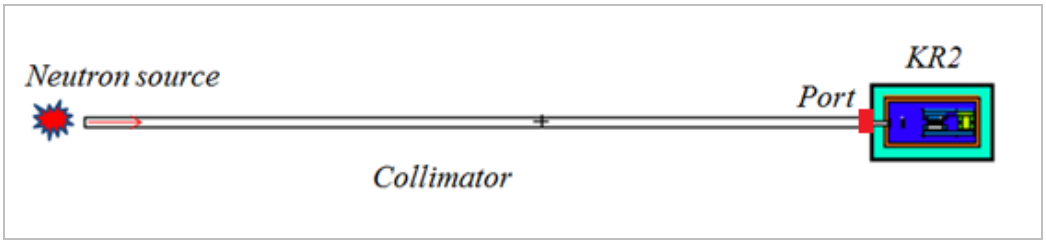

Fig. 24 *The MCNPX model of collimator coupled to the KR2 box*

With this model the neutron spectra were calculated at the KR2 port as well as over the Si active layer. The result of this calculation is shown in Fig.25. The blue curve corresponds to neutrons which reached the external port of KR2 and the red one corresponds to neutrons which reached the Si layer.

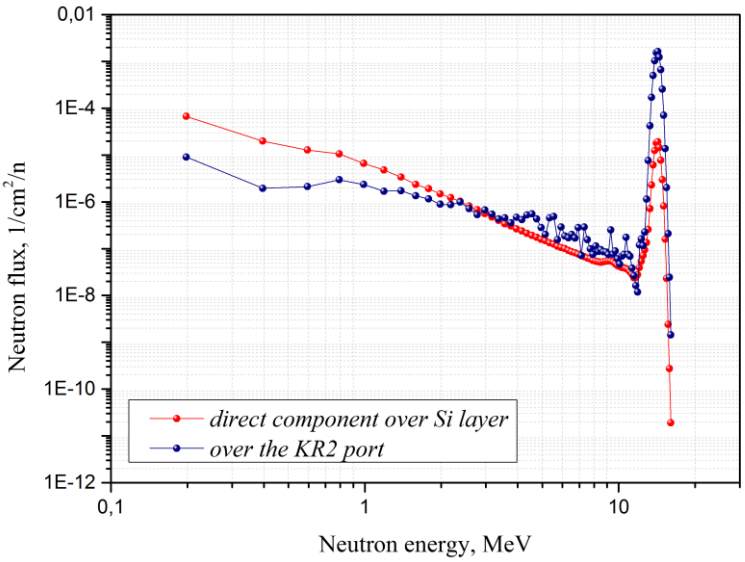

Fig. 25 *Neutron spectra calculated with a point source (En= 14 MeV)*

Second step: After spectra normalization the comparison of obtained fluxes at the Si detector position is shown in Fig.26. The red curve represents the fast neutron direct component. It could be seen that this fraction is small by comparison to the total neutron flux expected at the detector position.

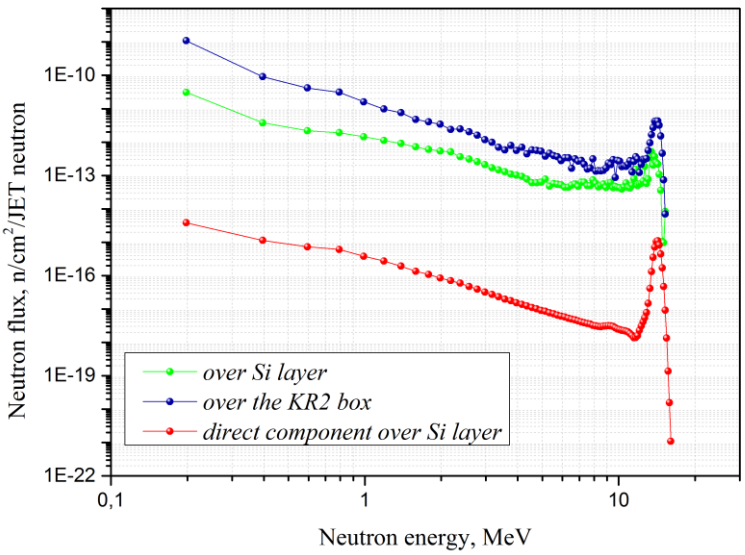

Fig. 26 *Comparison between the DT neutron spectra calculated*

VII. Conclusions

Neutron spectra for the JET KR2 diagnostic were simulated using MCNPX for typical JET DT and DD scenarios. Spectra were obtained for two KR2 locations, namely Octant 3 and Octant 8. All data with indicated errors are summarized in Tables 2-6. All these calculations are based on already existing model of the JET Torus Hall, supplementing by detailed modeling of the KR2 diagnostic. Any inaccuracies in that model propagate into the model described here.

The energy deposition in the Si layer has also been studied. It is confirmed that neutrons and gamma-rays can affect the active silicon detector and contribute to a background signal. Unfortunately this is unavoidable with the current radiation shield configuration. Moreover, the highest contribution is in the low energy range exactly in the working range of the NPA.

Calculations with different thicknesses of the active silicon detector were performed and possible neutron background was evaluated. These results can contribute to the selection of the detector thickness. In this context it is also important to pay attention to the full design of the detector since the active Silicon layer is normally mounted on a substrate which can give an additional background contribution. Some first results on this effect are presented in this report.

The current configuration of the shielding attenuates neutrons and could reduce neutron flux up to 10 times for DT neutrons and more than 20 times for the DD case. If placed in Octant 8, the neutron flux is going to be higher due to the more exposed position with respect to the torus vessel.

In addition the gamma flux distributions were simulated as well. Those gamma-rays are caused by neutron interactions with shield material mostly via the neutron capture reaction channel. It is shown that mainly they are absorbed by radiation shielding but the part which can reach the detector region may influence the background level.

References

[1] V.I. Afanasyev, *"Neutral particle analyzer/isotope separator for measurement of hydrogen isotope composition of JET plasmas",* Review of Scientific Instruments, Vol 74, N.4, 2003, pp 2338-2352

[2] D.B.Pelowitz, M*CNPX Users Manual* Version2.5.0—LA-CP05-0369, LosAlamos National LaboratoryLACP,2005.

[3] M. Gatu Johnson et al, Nucl. Instr. Meth. A, 591, 2, p417-430 (2008)

[4] Ziegler, J., 1980. *Handbook of Stopping Cross-Sections for Energetic Ions in all Elements*, 5, Pergamon Press, New York.

[5] http://www.nndc.bnl.gov/qcalc/ (online)

VIII. Data tables

Table 2. Neutron spectra calculated for DT scenario (Oct3)

Neutron energy (MeV)	dN_n/dE at Si area (n/cm^2/JET neutron)	Error, %	dN_n/dE at KR2 box (n/cm^2/JET neutron)	Error, %	dN_n/dE at "Interior" (n/cm^2/JET neutron)	Error, %	dN_γ/dE at Si area (γ/cm^2/JET neutron)	Error, %	dN_γ/dE at "Interior" (γ/cm^2/JET neutron)	Error, %
0,19802	3,08E-11	7,37	1,08E-09	4,50E-01	3,47E-11	4,14	4,79E-12	4,4	1,58E-12	3,34
0,39604	3,78E-12	12,54	9,09E-11	1,58E+00	2,85E-12	10,33	6,22E-12	4,16	2,14E-12	3,41
0,59406	2,20E-12	6,25	4,16E-11	2,34E+00	1,85E-12	6,15	1,21E-11	3,26	2,36E-12	2,86
0,79208	1,92E-12	6,39	3,12E-11	2,75E+00	1,59E-12	5,36	1,79E-12	4,3	1,02E-12	2,93
0,9901	1,45E-12	6,29	1,61E-11	3,81E+00	1,33E-12	9,05	2,32E-12	5,4	1,20E-12	3,4
1,1881	1,12E-12	5,96	9,81E-12	4,92E+00	9,85E-13	4,96	1,36E-12	4,71	8,14E-13	2,48
1,3861	9,12E-13	5,94	7,58E-12	5,65E+00	8,15E-13	4,92	1,66E-12	5,02	8,55E-13	2,82
1,5842	7,24E-13	6,32	4,79E-12	6,85E+00	6,69E-13	4,9	1,25E-12	4,8	6,98E-13	2,7
1,7822	6,03E-13	6,53	4,04E-12	7,72E+00	5,69E-13	4,96	1,02E-12	4,08	5,96E-13	2,05
1,9802	5,44E-13	7,1	3,43E-12	8,50E+00	4,85E-13	4,98	7,41E-13	4,86	4,61E-13	2,1
2,1782	5,09E-13	16,24	2,41E-12	9,31E+00	4,24E-13	5,93	6,38E-13	4,31	4,07E-13	1,95
2,3762	3,61E-13	6,56	2,50E-12	9,31E+00	3,51E-13	4,93	1,16E-12	5,1	8,34E-13	1,4
2,5743	3,11E-13	7,12	2,05E-12	1,01E+01	2,86E-13	4,95	3,97E-13	5,68	2,20E-13	2,83
2,7723	2,60E-13	7,54	1,62E-12	1,10E+01	2,42E-13	5,42	4,97E-13	4,99	3,30E-13	3,3
2,9703	2,11E-13	7,66	1,17E-12	1,27E+01	2,38E-13	21,36	3,42E-13	5,74	1,80E-13	2,45
3,1683	1,71E-13	8,06	9,84E-13	1,49E+01	1,52E-13	5,04	3,44E-13	5,99	1,65E-13	2,65
3,3663	1,48E-13	7,81	6,96E-13	1,84E+01	1,26E-13	5,07	3,17E-13	5,73	1,67E-13	2,67
3,5644	1,29E-13	11,06	5,79E-13	1,95E+01	1,10E-13	5,42	2,89E-13	5,14	1,50E-13	2,7
3,7624	1,10E-13	9,19	7,96E-13	1,89E+01	9,28E-14	5,28	1,86E-13	7,04	9,68E-14	2,87
3,9604	1,03E-13	8,63	5,66E-13	1,75E+01	8,13E-14	5,53	2,12E-13	5,92	1,13E-13	2,69
4,1584	9,32E-14	9,97	6,96E-13	1,76E+01	6,95E-14	5,45	1,68E-13	7,8	9,30E-14	3
4,3564	7,77E-14	9,69	4,46E-13	2,28E+01	6,05E-14	5,22	2,77E-13	5,58	1,22E-13	2,61
4,5545	6,09E-14	10,56	5,82E-13	2,12E+01	5,67E-14	6,44	1,62E-13	7,89	7,93E-14	2,97
4,7525	6,04E-14	10,71	5,59E-13	1,93E+01	5,12E-14	6,05	1,52E-13	9,32	7,28E-14	2,92
4,9505	6,30E-14	10,01	5,36E-13	2,21E+01	4,60E-14	5,35	2,14E-13	6,46	8,40E-14	2,84
5,1485	7,80E-14	21	3,79E-13	2,48E+01	4,48E-14	5,3	1,06E-13	10,47	5,53E-14	3,09
5,3465	4,76E-14	11,33	4,64E-13	2,31E+01	4,29E-14	5,39	1,38E-13	10,27	5,99E-14	3,01
5,5446	5,68E-14	10,99	3,92E-13	2,47E+01	4,15E-14	5,96	1,07E-13	8,62	4,64E-14	3,19
5,7426	5,45E-14	10,22	3,66E-13	2,46E+01	4,13E-14	5,58	1,06E-13	9,93	4,36E-14	3,3
5,9406	5,19E-14	12,89	2,80E-13	2,58E+01	4,80E-14	10,82	2,82E-13	6,1	1,12E-13	2,48
6,1386	4,42E-14	11,48	3,37E-13	2,80E+01	4,02E-14	6,54	3,55E-13	5,01	1,40E-13	2,4
6,3366	4,47E-14	12,18	3,37E-13	2,70E+01	4,45E-14	12,6	6,07E-14	10,7	2,65E-14	3,85

6,5347	5,14E-14	10,98	1,65E-13	3,60E+01	3,77E-14	5,16	8,53E-14	12,75	3,13E-14	5,88
6,7327	5,48E-14	22,63	3,16E-13	2,58E+01	3,89E-14	6,65	7,93E-14	11,29	3,51E-14	3,07
6,9307	4,67E-14	10,43	2,67E-13	2,98E+01	3,71E-14	5,22	9,24E-14	8,43	4,38E-14	2,79
7,1287	6,23E-14	13,37	2,80E-13	2,84E+01	4,27E-14	8,82	6,53E-14	8,4	3,19E-14	3,12
7,3267	6,24E-14	29,91	2,16E-13	3,39E+01	3,95E-14	9,15	1,66E-13	6,89	6,86E-14	2,49
7,5248	4,96E-14	12,69	1,55E-13	3,66E+01	3,95E-14	8,23	1,49E-13	6,28	1,62E-13	2,47
7,7228	4,96E-14	12,13	1,66E-13	3,54E+01	4,14E-14	7,93	1,44E-12	3,26	5,63E-13	2,58
7,9208	7,38E-14	31,76	3,14E-13	3,02E+01	4,36E-14	13,74	6,41E-14	14,28	3,75E-14	2,86
8,1188	5,80E-14	12,27	1,35E-13	4,08E+01	4,33E-14	13,23	5,89E-14	8,91	2,40E-14	3,06
8,3168	4,51E-14	14,83	1,39E-13	3,47E+01	3,91E-14	8,75	1,53E-14	14,57	9,28E-15	3,96
8,5149	5,03E-14	10,88	1,36E-13	3,14E+01	3,98E-14	7,19	2,37E-14	21,87	6,80E-15	4,75
8,7129	5,53E-14	17,47	1,42E-13	3,57E+01	4,91E-14	15,86	9,25E-14	8,47	3,58E-14	2,61
8,9109	4,35E-14	11,94	1,66E-13	3,81E+01	3,85E-14	6,52	2,01E-13	8,01	7,02E-14	2,53
9,1089	5,97E-14	30,92	2,36E-13	3,57E+01	4,63E-14	19,05	8,57E-14	8,51	3,46E-14	2,64
9,3069	6,14E-14	13,04	2,12E-13	3,34E+01	6,96E-14	23,29	1,10E-13	7,27	3,95E-14	2,6
9,505	4,32E-14	11,61	2,99E-13	3,13E+01	5,41E-14	20,1	7,56E-15	55,41	9,95E-16	12,96
9,703	4,69E-14	13,33	8,72E-14	4,26E+01	4,13E-14	11,41	2,59E-15	45,99	6,61E-16	14,57
9,901	4,38E-14	12,01	2,81E-13	3,04E+01	3,75E-14	9,15	3,02E-15	37,51	8,81E-16	9,93
10,099	4,29E-14	13,85	2,67E-13	3,44E+01	4,00E-14	16,12	1,80E-15	70,69	5,41E-16	14,74
10,297	3,95E-14	12,1	1,82E-13	3,77E+01	4,15E-14	23,46	8,65E-16	57,91	2,90E-16	14,68
10,495	4,55E-14	13,12	1,94E-13	3,52E+01	4,31E-14	20,6	0	0	3,01E-16	20,54
10,693	5,92E-14	19,66	1,85E-13	3,10E+01	5,18E-14	23,69	1,45E-15	68,9	1,28E-16	26,19
10,891	4,40E-14	11,31	2,16E-13	3,22E+01	3,39E-14	6,04	1,38E-15	83,97	1,24E-16	24,89
11,089	4,25E-14	11,72	2,75E-13	2,73E+01	3,58E-14	6,34	1,20E-16	100	4,91E-17	29,66
11,287	5,12E-14	12,64	1,27E-13	2,91E+01	4,60E-14	12,97	0	0	6,66E-17	32,41
11,485	8,01E-14	27,05	2,62E-13	2,89E+01	7,09E-14	24,35	2,69E-16	100	4,37E-17	33,17
11,683	1,53E-13	74,34	3,65E-13	2,75E+01	5,31E-14	17,18	0	0	4,58E-17	39,97
11,881	4,98E-14	11,42	3,12E-13	3,20E+01	5,11E-14	20,2	0	0	1,14E-17	52,5
12,079	5,49E-14	12,85	1,23E-13	3,39E+01	4,41E-14	15,62	5,71E-16	84,24	7,09E-18	57,51
12,277	5,89E-14	12,64	2,17E-13	3,11E+01	5,72E-14	29,9	0	0	2,90E-17	49,24
12,475	6,77E-14	13,23	3,02E-13	2,83E+01	7,18E-14	24,08	0	0	1,22E-19	100
12,673	1,88E-13	70,88	3,01E-13	2,91E+01	5,96E-14	16,44	0	0	1,82E-17	74,06
12,871	5,69E-14	14,11	3,21E-13	2,68E+01	6,34E-14	24,83	0	0	6,16E-18	100
13,069	7,77E-14	30,81	5,61E-13	2,38E+01	7,44E-14	19,38	0	0	3,03E-18	98,65
13,267	3,33E-13	51,13	9,43E-13	1,87E+01	1,28E-13	17,73	0	0	2,97E-18	83,75
13,465	5,18E-13	45,25	1,67E-12	1,30E+01	2,69E-13	18,12	0	0	8,50E-18	72,22
13,663	2,03E-13	22,68	2,70E-12	1,08E+01	2,37E-13	18,08	4,16E-16	100	2,55E-17	51,89
13,861	3,68E-13	44,23	4,23E-12	8,61E+00	4,86E-13	15,02	0	0	6,94E-18	67,64
14,059	2,44E-13	20,74	4,28E-12	8,88E+00	5,89E-13	20,21	0	0	0	0
14,257	2,18E-13	23,37	4,27E-12	8,86E+00	5,30E-13	23,84	0	0	1,42E-17	57,22
14,455	1,09E-13	32,88	3,20E-12	1,01E+01	2,85E-13	21,89	0	0	2,58E-17	56,01
14,653	3,58E-14	71,32	1,52E-12	1,54E+01	1,31E-13	34,58	0	0	2,55E-18	71,59
14,851	1,07E-15	71,14	4,60E-13	2,74E+01	1,95E-14	74,14	0	0	9,64E-18	51,76

Table 3. Neutron spectra calculated for DD scenario (Oct3)

Neutron energy (MeV)	dN_n/dE at Si area (n/cm^2/JET neutron)	Error, %	dN_n/dE at KR2 box (n/cm^2/JET neutron)	Error, %	dN_n/dE at "Interior" (n/cm^2/JET neutron)	Error, %	dN_γ/dE at Si area (γ/cm^2/JET neutron)	Error, %	dN_γ/dE at "Interior" (γ/cm^2/JET neutron)	Error, %
0,04951	1,43E-11	9,32	8,24E-10	0,4	1,72E-11	5,36	1,92E-14	17,51	1,54E-14	2,64
0,09901	5,61E-13	17,64	7,27E-11	1,38	4,88E-13	26,06	2,10E-13	7,06	2,60E-13	2,3
0,14851	3,52E-13	20,17	4,82E-11	1,67	4,07E-13	35,3	8,50E-13	5,13	2,33E-13	3,08
0,19802	2,82E-13	25,08	3,44E-11	1,98	2,55E-13	34,53	1,17E-12	5,69	3,16E-13	3,15
0,24752	2,40E-13	33,23	2,53E-11	2,35	2,69E-13	43,04	9,10E-13	5,82	3,23E-13	3,07
0,29703	1,35E-13	33,03	2,17E-11	2,52	1,09E-13	30,6	8,09E-13	5,76	2,84E-13	2,96
0,34653	1,14E-13	19,27	1,97E-11	2,7	1,19E-13	38,01	6,57E-13	6,67	2,42E-13	2,84
0,39604	9,03E-14	18,69	1,35E-11	3,27	6,53E-14	14,83	6,46E-13	6,8	2,41E-13	2,71
0,44554	8,72E-14	23,54	8,59E-12	4,07	6,33E-14	24,14	4,70E-13	5,88	2,02E-13	2,63
0,49505	9,30E-14	23,4	9,70E-12	3,82	6,98E-14	26,62	4,50E-12	4,43	2,08E-13	2,5
0,54455	1,24E-13	38,82	9,07E-12	3,95	7,03E-14	24,21	1,13E-12	5,55	6,86E-13	2,14
0,59406	1,24E-13	27,11	8,75E-12	4,07	1,28E-13	49,42	2,80E-13	12,26	1,37E-13	2,47
0,64356	1,51E-13	48,97	8,53E-12	4,14	9,92E-14	37,13	2,41E-13	7,23	1,26E-13	2,17
0,69307	8,19E-14	24,28	7,00E-12	4,69	1,22E-13	49,55	2,34E-13	6,09	1,37E-13	2,18
0,74257	6,33E-14	25,45	6,40E-12	4,73	1,14E-13	54,39	2,28E-13	10,5	1,31E-13	2,09
0,79208	6,00E-14	34,59	4,73E-12	5,43	6,58E-14	41,78	1,95E-13	7,16	1,23E-13	2,15
0,84158	5,69E-14	29,39	4,36E-12	5,77	8,37E-14	47,2	2,31E-13	7,99	1,33E-13	2,36
0,89109	4,28E-14	26,14	3,45E-12	6,48	8,02E-14	65,39	2,84E-13	11,37	1,57E-13	5,22
0,94059	4,87E-14	28,2	2,93E-12	7,23	3,31E-14	19,31	1,90E-13	7,26	1,20E-13	1,91
0,9901	3,94E-14	23,14	2,76E-12	8,05	3,25E-14	21,08	2,15E-13	8,6	1,23E-13	1,94
1,0396	4,86E-14	41,04	2,20E-12	8,78	5,25E-14	54,34	2,37E-13	7,32	1,36E-13	2,09
1,0891	3,37E-14	25,81	1,86E-12	9,08	2,51E-14	21,62	1,64E-13	7,63	1,14E-13	1,79
1,1386	2,49E-14	21,29	1,75E-12	9,55	1,92E-14	11,24	1,44E-13	8,36	1,09E-13	1,7
1,1881	2,65E-14	23,25	2,31E-12	8,69	1,79E-14	11,36	1,67E-13	7,63	1,10E-13	1,73
1,2376	2,20E-14	22,43	1,52E-12	10,12	1,74E-14	11,32	1,28E-13	7,18	1,05E-13	1,66
1,2871	2,30E-14	41,17	1,41E-12	10,34	1,50E-14	11,54	1,71E-13	6,46	1,22E-13	2,2
1,3366	2,45E-14	28,35	9,61E-13	12,76	1,54E-14	12,95	2,69E-13	7,52	1,47E-13	2,67
1,3861	1,60E-14	29,25	1,23E-12	11,27	1,73E-14	14,84	1,82E-13	9,39	1,14E-13	2,3
1,4356	3,23E-14	49,5	1,07E-12	12,17	1,75E-14	18,05	1,93E-13	9,86	1,13E-13	3,02
1,4851	3,12E-14	39,19	8,24E-13	13,68	1,97E-14	21,87	1,65E-13	7,86	1,09E-13	2,54
1,5347	3,24E-14	38,62	8,64E-13	12,85	2,25E-14	24,99	1,31E-13	11,09	9,15E-14	1,63
1,5842	4,53E-14	34,78	5,55E-13	15,58	2,53E-14	29,29	1,12E-13	7,41	8,35E-14	1,41
1,6337	3,28E-14	37,38	7,73E-13	14,28	2,41E-14	35,78	1,46E-13	6,29	9,87E-14	1,55
1,6832	1,46E-14	27,33	1,03E-12	12,62	1,62E-14	23,54	1,36E-13	8,88	8,62E-14	1,48
1,7327	1,63E-14	36,2	1,06E-12	12,5	1,73E-14	39,45	1,50E-13	7,37	9,67E-14	1,59
1,7822	1,20E-14	34,15	7,04E-13	15,54	1,30E-14	26,65	2,05E-13	34,58	8,52E-14	1,5
1,8317	1,33E-14	44,37	6,01E-13	15,66	7,16E-14	82,36	9,04E-14	9,74	7,28E-14	1,45
1,8812	1,92E-14	49,88	4,66E-13	18,56	1,39E-14	39,41	1,02E-13	9,5	7,30E-14	1,43
1,9307	3,23E-14	68,5	4,06E-13	19,44	2,43E-14	65,49	9,07E-14	10,05	6,81E-14	1,36
1,9802	1,61E-14	55,04	4,19E-13	19,07	1,94E-14	55,7	9,36E-14	9,44	7,09E-14	1,46
2,0297	3,18E-15	26,62	5,07E-13	19,43	7,63E-15	12,36	7,80E-14	8,65	6,39E-14	1,43
2,0792	7,49E-15	29,13	5,62E-13	17,73	6,90E-15	13,71	8,47E-14	9,02	6,22E-14	1,39

2,1287	4,70E-15	25,6	7,04E-13	16,39	8,42E-15	13,02	8,96E-14	8,73	6,72E-14	1,47
2,1782	1,82E-14	47	6,04E-13	17,12	9,03E-15	13,61	7,99E-14	8,33	6,52E-14	1,51
2,2277	1,12E-14	32,42	9,09E-13	15,17	9,83E-15	16,6	6,00E-13	3,47	5,34E-13	1,08
2,2772	1,11E-14	29,18	6,43E-13	15,7	1,08E-14	21,3	4,69E-14	12,19	3,14E-14	2,2
2,3267	1,37E-14	36,94	8,33E-13	15,69	1,60E-14	27,43	5,67E-14	10,13	3,19E-14	2,22
2,3762	1,54E-14	36,21	8,69E-13	14,44	2,28E-14	34,55	4,46E-14	12,1	2,81E-14	2,15
2,4257	2,75E-14	64,98	1,28E-12	12,78	1,56E-14	28,49	5,02E-14	11,3	3,12E-14	2,32
2,4752	1,66E-14	44,72	1,01E-12	14,28	1,79E-14	29,06	4,96E-14	13,73	2,65E-14	2,16
2,5248	9,19E-15	34,17	8,66E-13	14,87	6,21E-14	79,86	4,36E-14	12,92	2,65E-14	2,09
2,5743	7,41E-15	57,36	8,76E-13	15,37	5,46E-15	26,6	5,85E-14	30,36	2,65E-14	2,11
2,6238	5,14E-16	59,15	4,32E-13	22,87	4,64E-15	33,85	4,20E-14	12,89	2,68E-14	2,13
2,6733	6,85E-16	50,87	2,61E-13	29,62	2,18E-15	39,44	4,51E-14	11,21	2,75E-14	2,24

Table 4. Neutron spectra calculated for DT scenario (Oct8)

Neutron energy (MeV)	dN_n/dE at Si area (n/cm^2/JET neutron)	Error, %	dN_n/dE at KR2 box (n/cm^2/JET neutron)	Error, %	dN_n/dE at "Interior" (n/cm^2/JET neutron)	Error, %	dN_γ/dE at Si area (γ/cm^2/JET neutron)	Error, %	dN_γ/dE at "Interior" (γ/cm^2/JET neutron)	Error, %
0,19802	1,32E-10	1,48	1,40E-09	0,29	1,47E-10	1,23	2,07E-11	1,89	6,17E-12	1,31
0,39604	2,11E-11	1,76	1,49E-10	0,94	1,68E-11	1,56	2,65E-11	1,64	8,55E-12	1,32
0,59406	1,49E-11	1,98	7,75E-11	1,32	1,26E-11	1,47	4,94E-11	1,5	9,34E-12	1,22
0,79208	1,35E-11	1,82	6,31E-11	1,46	1,16E-11	1,49	7,80E-12	1,84	4,04E-12	1,27
0,9901	9,51E-12	2,15	3,50E-11	1,99	8,47E-12	1,47	1,07E-11	1,97	4,79E-12	1,35
1,1881	7,63E-12	1,96	2,13E-11	2,57	6,84E-12	1,46	5,38E-12	4,5	2,64E-12	1,14
1,3861	6,12E-12	2,08	1,60E-11	2,92	5,57E-12	1,45	6,83E-12	1,96	2,96E-12	1,23
1,5842	4,95E-12	3,36	1,31E-11	3,31	4,52E-12	1,45	5,28E-12	2,02	2,42E-12	1,21
1,7822	3,99E-12	2,26	1,02E-11	3,73	3,77E-12	1,64	3,77E-12	1,96	1,97E-12	1,06
1,9802	3,39E-12	3,12	7,54E-12	4,27	3,09E-12	1,44	2,83E-12	2,58	1,55E-12	1,11
2,1782	2,76E-12	2,58	6,65E-12	4,44	2,61E-12	1,44	2,28E-12	2,32	1,27E-12	1,05
2,3762	2,37E-12	2,61	6,63E-12	4,43	2,21E-12	1,45	3,40E-12	2,63	2,01E-12	0,8
2,5743	1,97E-12	3,33	5,97E-12	4,69	1,82E-12	1,44	1,73E-12	2,63	1,02E-12	1,29
2,7723	1,58E-12	2,66	3,97E-12	5,4	1,49E-12	1,45	2,13E-12	2,7	1,30E-12	1,3
2,9703	1,38E-12	3,47	3,42E-12	6,06	1,22E-12	1,46	1,35E-12	3,98	6,41E-13	1,19
3,1683	1,19E-12	3,62	3,33E-12	6,34	9,96E-13	1,47	1,32E-12	3,2	5,75E-13	1,21
3,3663	1,03E-12	6,15	2,66E-12	7,34	8,49E-13	1,49	1,39E-12	2,94	5,68E-13	1,22
3,5644	8,00E-13	3,63	2,03E-12	8,32	6,99E-13	1,48	1,25E-12	3,05	5,21E-13	1,23
3,7624	7,34E-13	3,85	1,91E-12	8,47	6,19E-13	1,62	8,01E-13	3,67	3,84E-13	1,33
3,9604	6,56E-13	4,12	1,64E-12	9,44	5,38E-13	1,53	8,53E-13	3,23	4,20E-13	1,3
4,1584	5,56E-13	4,14	1,77E-12	9,01	4,59E-13	1,52	6,38E-13	3,39	3,31E-13	1,34
4,3564	5,30E-13	5,06	1,40E-12	9,9	4,16E-13	1,67	1,08E-12	4,47	4,38E-13	1,21
4,5545	4,67E-13	4,26	1,41E-12	9,98	3,65E-13	1,7	7,04E-13	3,81	2,97E-13	1,3
4,7525	4,22E-13	4,28	1,32E-12	9,97	3,35E-13	1,69	7,27E-13	7,55	2,66E-13	1,33
4,9505	3,77E-13	4,35	1,62E-12	9,27	3,03E-13	1,78	1,04E-12	24,23	3,03E-13	1,28
5,1485	3,70E-13	5,78	1,24E-12	10,2	2,87E-13	1,66	4,73E-13	5,68	1,96E-13	1,43

5,3465	3,74E-13	5,03	1,10E-12	10,87	2,98E-13	2,17	5,25E-13	4,67	2,24E-13	1,34
5,5446	3,99E-13	5,91	1,10E-12	11,1	2,95E-13	2,2	4,06E-13	4,6	1,83E-13	1,4
5,7426	3,33E-13	4,58	1,25E-12	11,4	2,84E-13	2,02	4,12E-13	5,41	1,63E-13	1,41
5,9406	3,68E-13	7,34	1,06E-12	11,32	2,77E-13	2	1,07E-12	3,17	4,05E-13	1,15
6,1386	4,15E-13	11,32	7,66E-13	13,11	2,83E-13	2,21	1,33E-12	2,67	4,93E-13	1,11
6,3366	3,38E-13	4,58	9,80E-13	12,55	2,84E-13	2,06	2,52E-13	5,74	1,10E-13	1,57
6,5347	3,24E-13	4,48	7,91E-13	14,1	2,86E-13	2,52	2,97E-13	6,49	1,11E-13	1,51
6,7327	3,36E-13	5,11	5,87E-13	15,73	2,83E-13	2,4	2,90E-13	4,85	1,27E-13	1,42
6,9307	3,17E-13	4,78	6,13E-13	14,7	2,70E-13	2,8	3,74E-13	5,73	1,73E-13	1,28
7,1287	3,63E-13	6,47	5,74E-13	16,1	2,75E-13	3,02	3,19E-13	5,89	1,16E-13	1,4
7,3267	3,24E-13	5,5	4,73E-13	18,12	2,64E-13	2,69	6,00E-13	4,85	2,47E-13	1,14
7,5248	3,21E-13	6,25	5,90E-13	17,04	2,62E-13	2,65	7,00E-13	3,78	7,12E-13	1,09
7,7228	3,50E-13	7,4	5,23E-13	17,53	2,67E-13	4,04	5,65E-12	3,6	1,94E-12	1,03
7,9208	3,70E-13	15,85	5,02E-13	16,3	2,59E-13	3,04	2,57E-13	5,37	1,46E-13	1,26
8,1188	2,87E-13	4,67	5,11E-13	17,86	2,64E-13	3,61	2,80E-13	9,32	9,00E-14	1,39
8,3168	3,15E-13	4,49	4,65E-13	16,79	2,57E-13	3,2	1,08E-13	8,9	3,77E-14	1,82
8,5149	2,93E-13	4,68	4,54E-13	16,28	2,45E-13	2,27	8,75E-14	11,36	3,05E-14	1,95
8,7129	3,45E-13	5,72	6,23E-13	16,8	2,56E-13	3,22	3,92E-13	4,64	1,31E-13	1,22
8,9109	3,21E-13	6,94	5,78E-13	16,95	2,72E-13	3,69	7,03E-13	3,69	2,51E-13	1,14
9,1089	3,16E-13	4,59	5,79E-13	15,35	2,68E-13	3,75	3,81E-13	4,33	1,29E-13	1,22
9,3069	3,14E-13	4,23	5,21E-13	18,56	2,56E-13	2,81	4,20E-13	4,8	1,43E-13	1,18
9,505	3,26E-13	4,82	6,31E-13	16,53	2,77E-13	4,01	1,42E-14	19,3	6,64E-15	3,7
9,703	3,51E-13	5,99	6,17E-13	17,63	2,88E-13	4,32	9,87E-15	23,07	5,55E-15	4
9,901	3,06E-13	4,65	5,88E-13	15,8	2,90E-13	4,68	2,66E-14	29,52	6,91E-15	3,49
10,099	3,66E-13	10,05	5,79E-13	16,62	2,63E-13	2,43	1,15E-14	32,08	5,46E-15	3,89
10,297	3,03E-13	4,26	5,55E-13	17,42	2,67E-13	4,25	5,09E-15	35,56	4,40E-15	4,43
10,495	3,33E-13	4,35	5,37E-13	17,3	2,59E-13	3,88	7,60E-15	23,62	3,77E-15	4,64
10,693	3,50E-13	7,06	8,92E-13	14,09	2,71E-13	3,76	3,33E-15	32,83	3,45E-15	4,84
10,891	3,50E-13	5,62	6,37E-13	14,98	2,96E-13	4,66	2,94E-15	43,07	1,88E-15	5,78
11,089	3,30E-13	5,14	7,24E-13	13,81	3,16E-13	5,73	1,76E-15	71,73	3,44E-16	12,5
11,287	3,32E-13	4,46	7,27E-13	14,61	3,00E-13	4,21	4,38E-16	100	2,02E-16	17,4
11,485	3,42E-13	5,23	6,57E-13	15,04	3,09E-13	5,15	2,82E-16	100	1,22E-16	20,49
11,683	3,55E-13	10,8	5,61E-13	15,62	2,98E-13	3,49	6,19E-16	71,82	1,26E-16	20,67
11,881	4,39E-13	17,38	6,28E-13	14,93	3,17E-13	4,98	3,27E-16	100	8,98E-17	24,8
12,079	3,90E-13	20,42	6,90E-13	14,14	3,00E-13	3,84	0	0	6,95E-17	24,88
12,277	3,58E-13	4,34	7,47E-13	13,38	3,27E-13	4,51	0	0	2,10E-17	44,4
12,475	3,90E-13	4,99	7,94E-13	13,31	3,47E-13	4,29	0	0	6,19E-18	58,1
12,673	3,90E-13	5,15	9,11E-13	12,9	3,64E-13	4,37	2,84E-16	100	1,08E-17	62,19
12,871	4,54E-13	10,7	9,42E-13	13,07	3,76E-13	4,4	0	0	2,60E-17	39,8
13,069	4,58E-13	7,03	1,02E-12	13,03	4,45E-13	5,9	0	0	9,75E-18	77,34
13,267	6,80E-13	19,72	2,28E-12	9,2	5,26E-13	6,1	0	0	3,33E-18	97,85
13,465	9,37E-13	15,94	5,71E-12	6,13	1,07E-12	7,29	0	0	1,37E-17	65,54
13,663	1,61E-12	11,86	1,39E-11	4,05	2,09E-12	6,17	0	0	8,08E-18	70,71
13,861	2,68E-12	11,55	2,65E-11	3	3,49E-12	4,41	0	0	2,51E-18	78,41
14,059	4,41E-12	11,52	3,77E-11	2,52	4,84E-12	4,13	0	0	2,54E-17	59,15

14,257	3,81E-12	12,73	3,94E-11	2,48	4,42E-12	4,28	0	0	4,81E-18	84,48
14,455	2,55E-12	15,1	3,07E-11	2,82	3,35E-12	4,53	0	0	1,00E-17	72,32
14,653	1,21E-12	23,78	1,61E-11	3,92	1,73E-12	6,44	0	0	2,56E-17	44,87
14,851	7,30E-13	32,19	6,74E-12	6,1	7,38E-13	9,95	0	0	1,94E-17	53,96
15,05	4,31E-13	48,18	1,74E-12	11,92	1,97E-13	18,89	0	0	2,50E-17	35,81
15,248	3,69E-14	58,17	3,61E-13	25,38	4,84E-14	34,69	0	0	3,93E-17	39,07

Table 5. Neutron spectra calculated for DD scenario (Oct8)

Neutron energy (MeV)	dN_n/dE at Si area (n/cm^2/JET neutron)	Error, %	dN_n/dE at KR2 box (n/cm^2/JET neutron)	Error %	dN_n/dE at "Interior" (n/cm^2/JET neutron)	Error %	dN_γ/dE at Si area (γ/cm^2/JET neutron)	Error %	dN_γ/dE at "Interior" (γ/cm^2/JET neutron)	Error %
0,04951	3,11E-11	2,96	1,06E-09	0,36	4,58E-11	1,77	5,75E-14	10,27	3,62E-14	1,57
0,09901	1,51E-12	7,83	1,17E-10	1,12	1,18E-12	12,2	5,88E-13	4,89	5,95E-13	1,25
0,14851	1,07E-12	7,49	8,27E-11	1,33	8,05E-13	8,87	2,24E-12	3,01	5,55E-13	1,57
0,19802	8,09E-13	6,14	5,92E-11	1,59	5,98E-13	4,18	2,93E-12	2,52	7,64E-13	1,54
0,24752	7,15E-13	6,22	4,39E-11	1,84	5,28E-13	5,45	2,56E-12	2,88	7,72E-13	1,6
0,29703	6,27E-13	8,43	4,11E-11	1,93	4,73E-13	6,72	1,90E-12	2,75	6,74E-13	1,52
0,34653	6,21E-13	10,55	3,50E-11	2,11	5,38E-13	14,94	1,45E-12	3,06	5,71E-13	1,49
0,39604	5,37E-13	9,09	2,53E-11	2,48	4,85E-13	20,68	1,46E-12	3,08	5,71E-13	1,36
0,44554	4,19E-13	8,41	1,90E-11	2,95	3,04E-13	6,26	1,16E-12	3,57	4,64E-13	1,37
0,49505	4,35E-13	9,38	2,05E-11	2,8	3,48E-13	13,29	1,40E-11	2,08	4,89E-13	1,29
0,54455	4,07E-13	6,27	2,19E-11	2,72	3,30E-13	3,63	2,91E-12	2,34	1,62E-12	1
0,59406	4,30E-13	10,01	2,09E-11	2,82	3,25E-13	4,24	6,12E-13	4,32	3,04E-13	1,45
0,64356	4,31E-13	6,57	1,94E-11	2,84	3,38E-13	4,6	4,82E-13	4,32	2,73E-13	1,39
0,69307	3,41E-13	6,1	1,84E-11	3	2,83E-13	3,88	5,76E-13	3,81	3,03E-13	1,3
0,74257	3,10E-13	6,4	1,75E-11	3,04	2,54E-13	3,5	5,64E-13	9,33	2,72E-13	1,32
0,79208	2,71E-13	5,67	1,54E-11	3,28	2,36E-13	2,74	4,38E-13	4,79	2,72E-13	1,43
0,84158	2,71E-13	7,97	1,35E-11	3,58	2,21E-13	3,55	5,11E-13	3,99	2,95E-13	1,41
0,89109	2,55E-13	10,3	1,07E-11	4	2,04E-13	3,22	8,73E-13	5,95	3,99E-13	3,86
0,94059	2,63E-13	9,18	8,91E-12	4,48	2,21E-13	3,43	3,96E-13	4,39	2,56E-13	1,09
0,9901	2,37E-13	8,31	6,64E-12	5,21	1,97E-13	3,5	3,91E-13	4,43	2,50E-13	1,13
1,0396	2,42E-13	6,54	6,52E-12	5,28	1,81E-13	2,94	5,10E-13	4,23	2,78E-13	1,1
1,0891	1,94E-13	6,33	6,28E-12	5,37	1,75E-13	2,33	3,39E-13	4,85	2,29E-13	1,06
1,1386	1,88E-13	6,19	5,85E-12	5,57	1,68E-13	2,52	3,62E-13	7,96	2,18E-13	1,03
1,1881	2,11E-13	7,53	5,84E-12	5,53	1,65E-13	2,81	3,31E-13	5,31	2,18E-13	1,06
1,2376	2,05E-13	7,33	5,80E-12	5,42	1,65E-13	3,1	2,96E-13	5,56	2,11E-13	1,04
1,2871	1,86E-13	7,15	5,10E-12	5,78	1,54E-13	3,72	4,71E-13	4,79	2,52E-13	1,3
1,3366	1,89E-13	8,63	3,87E-12	6,89	1,55E-13	4,76	6,46E-13	3,95	3,18E-13	1,39
1,3861	2,11E-13	10,2	4,59E-12	6,23	1,72E-13	5,36	3,62E-13	4,59	2,28E-13	1,31
1,4356	2,20E-13	9,81	4,24E-12	6,43	1,72E-13	5,98	4,03E-13	5,33	2,43E-13	2,26
1,4851	2,25E-13	10,17	4,82E-12	6,17	1,75E-13	6,87	4,50E-13	5,78	2,29E-13	1,5
1,5347	2,47E-13	15,51	5,10E-12	6,16	1,80E-13	7,66	2,81E-13	5,56	1,82E-13	1,05
1,5842	1,97E-13	9,41	6,09E-12	5,83	2,18E-13	25,76	2,34E-13	5,75	1,63E-13	0,93

1,6337	1,38E-13	9,44	6,15E-12	5,93	1,89E-13	30,11	3,92E-13	6,32	2,09E-13	0,92
1,6832	1,22E-13	8,72	5,67E-12	6,12	1,20E-13	2,7	2,92E-13	5,3	1,82E-13	0,93
1,7327	1,18E-13	8,63	5,32E-12	6,25	1,06E-13	3,34	3,77E-13	4,4	2,05E-13	0,95
1,7822	1,03E-13	8,92	4,36E-12	6,68	1,02E-13	6,57	3,24E-13	6,61	1,75E-13	0,93
1,8317	1,13E-13	11,31	3,75E-12	7,17	1,08E-13	7,11	2,21E-13	7,1	1,49E-13	0,93
1,8812	1,16E-13	7,98	2,84E-12	8,16	1,04E-13	3,85	2,13E-13	5,39	1,43E-13	0,93
1,9307	9,94E-14	8,25	2,60E-12	8,37	1,49E-13	37,87	1,84E-13	6,22	1,38E-13	0,92
1,9802	9,97E-14	8,37	2,65E-12	8,11	9,18E-14	2,43	2,11E-13	5,16	1,44E-13	0,95
2,0297	1,08E-13	8,16	2,88E-12	7,69	9,81E-14	2,81	1,67E-13	6,14	1,31E-13	0,94
2,0792	1,08E-13	10,88	2,98E-12	7,5	8,66E-14	3,56	1,85E-13	6,53	1,26E-13	0,95
2,1287	1,10E-13	12,89	2,85E-12	7,87	9,94E-14	6,7	2,08E-13	5,36	1,37E-13	0,95
2,1782	1,37E-13	12,19	3,14E-12	7,71	1,20E-13	7,03	2,90E-13	24,02	1,32E-13	0,95
2,2277	1,46E-13	14,64	4,20E-12	7,01	1,30E-13	7,36	1,39E-12	4,2	1,11E-12	0,77
2,2772	1,75E-13	13,34	5,90E-12	6,15	1,98E-13	29,91	1,13E-13	7,54	6,13E-14	1,28
2,3267	2,05E-13	14,72	8,86E-12	5,21	1,73E-13	7,4	1,18E-13	8,22	6,29E-14	1,29
2,3762	2,38E-13	14,97	1,52E-11	4,03	3,33E-13	24,47	1,14E-13	10,63	5,53E-14	1,29
2,4257	2,49E-13	12,81	2,06E-11	3,48	3,36E-13	22,45	1,30E-13	7,87	6,32E-14	1,28
2,4752	1,87E-13	10,81	2,36E-11	3,27	2,85E-13	24,6	9,12E-14	10,29	5,20E-14	1,33
2,5248	1,22E-13	12,89	2,40E-11	3,25	2,72E-13	30,46	1,02E-13	9,47	5,29E-14	1,31
2,5743	7,33E-14	12,52	1,94E-11	3,61	8,85E-14	4,77	1,05E-13	8,45	5,26E-14	1,31
2,6238	4,81E-14	17,12	1,23E-11	4,56	5,92E-14	5,91	9,13E-14	7,64	5,35E-14	1,28
2,6733	2,22E-14	28,2	7,36E-12	5,91	3,49E-14	8,64	1,01E-13	7,98	5,57E-14	1,27
2,7228	2,06E-14	29,26	3,66E-12	8,37	1,70E-14	14,12	1,57E-13	8,47	6,64E-14	1,23
2,7723	8,36E-15	53,81	1,19E-12	14,5	6,43E-15	21,53	1,43E-13	7,05	6,93E-14	1,22
2,8218	4,95E-15	74,03	3,93E-13	25,32	2,80E-15	34,81	1,06E-13	7	6,21E-14	1,26

Table 6. Neutron and gamma energy deposition in 5 μm Silicon layer

Energy, MeV	Counts/n (neutron component)	Error	Counts/γ (gamma component)	Error	Counts / JET neutron over the whole detector (neutrons)	Counts / JET neutron over the whole detector (gammas)
0,0099	4,83E-09	0,5774	0,05103	1,00E-04	1,10E-15	1,09E-08
0,0198	4,03E-08	0,2	6,45E-06	0,0125	9,15E-15	1,38E-12
0,0297	3,51E-07	0,0677	2,00E-06	0,0224	7,98E-14	4,26E-13
0,0396	6,70E-07	0,049	6,41E-07	0,0395	1,52E-13	1,37E-13
0,04951	7,65E-07	0,0459	2,54E-07	0,0627	1,74E-13	5,42E-14
0,05941	6,85E-07	0,0485	1,04E-07	0,0981	1,56E-13	2,22E-14
0,06931	5,16E-07	0,0559	5,80E-08	0,1313	1,17E-13	1,24E-14
0,07921	3,93E-07	0,064	2,70E-08	0,1925	8,93E-14	5,77E-15
0,08911	3,09E-07	0,0722	2,40E-08	0,2041	7,03E-14	5,13E-15
0,09901	2,16E-07	0,0864	6,00E-09	0,4082	4,90E-14	1,28E-15
0,10891	1,58E-07	0,101	9,00E-09	0,3333	3,59E-14	1,92E-15
0,11881	1,19E-07	0,1162	1,00E-08	0,3162	2,71E-14	2,14E-15

0,12871	1,48E-07	0,1043	4,00E-09	0,5	3,37E-14	8,54E-16
0,13861	1,19E-07	0,1162	3,00E-09	0,5774	2,71E-14	6,41E-16
0,14851	9,34E-08	0,1313	9,00E-09	0,3333	2,12E-14	1,92E-15
0,15842	7,25E-08	0,1491	3,00E-09	0,5774	1,65E-14	6,41E-16
0,16832	7,25E-08	0,1491	2,00E-09	0,7071	1,65E-14	4,27E-16
0,17822	4,99E-08	0,1796	2,00E-09	0,7071	1,13E-14	4,27E-16
0,18812	4,51E-08	0,189	1,00E-09	1	1,02E-14	2,14E-16
0,19802	3,22E-08	0,2236	0	0	7,32E-15	0
0,20792	3,06E-08	0,2294	1,00E-09	1	6,95E-15	2,14E-16
0,21782	3,38E-08	0,2182	0	0	7,69E-15	0
0,22772	2,74E-08	0,2425	1,00E-09	1	6,22E-15	2,14E-16
0,23762	2,90E-08	0,2357	0	0	6,59E-15	0
0,24752	1,45E-08	0,3333	0	0	3,29E-15	0
0,25743	1,93E-08	0,2887	1,00E-09	1	4,39E-15	2,14E-16
0,26733	1,61E-08	0,3162	0	0	3,66E-15	0
0,27723	2,42E-08	0,2582	0	0	5,49E-15	0
0,28713	1,93E-08	0,2887	0	0	4,39E-15	0
0,29703	1,13E-08	0,378	0	0	2,56E-15	0
0,30693	1,13E-08	0,378	0	0	2,56E-15	0
0,31683	4,83E-09	0,5774	0	0	1,10E-15	0
0,32673	4,83E-09	0,5774	0	0	1,10E-15	0
0,33663	9,67E-09	0,4082	1,00E-09	1	2,20E-15	2,14E-16
0,34653	8,06E-09	0,4472	0	0	1,83E-15	0
0,35644	4,83E-09	0,5774	0	0	1,10E-15	0
0,36634	8,06E-09	0,4472	0	0	1,83E-15	0
0,37624	6,44E-09	0,5	0	0	1,46E-15	0
0,38614	8,06E-09	0,4472	0	0	1,83E-15	0
0,39604	1,13E-08	0,378	0	0	2,56E-15	0
0,40594	1,61E-09	1	0	0	3,66E-16	0
0,41584	3,22E-09	0,7071	0	0	7,32E-16	0
0,42574	8,06E-09	0,4472	0	0	1,83E-15	0
0,43564	1,61E-09	1	0	0	3,66E-16	0
0,44554	1,61E-09	1	0	0	3,66E-16	0
0,45545	6,44E-09	0,5	0	0	1,46E-15	0
0,46535	6,44E-09	0,5	0	0	1,46E-15	0
0,47525	4,83E-09	0,5774	0	0	1,10E-15	0
0,48515	0	0	0	0	0	0
0,49505	3,22E-09	0,7071	0	0	7,32E-16	0
0,50495	6,44E-09	0,5	0	0	1,46E-15	0
0,51485	4,83E-09	0,5774	0	0	1,10E-15	0
0,52475	4,83E-09	0,5774	0	0	1,10E-15	0
0,53465	0	0	0	0	0	0
0,54455	3,22E-09	0,7071	0	0	7,32E-16	0
0,55446	1,61E-09	1	0	0	3,66E-16	0
0,56436	0	0	0	0	0	0

0,57426	0	0	0	0	0	0
0,58416	3,22E-09	0,7071	0	0	7,32E-16	0
0,59406	4,83E-09	0,5774	0	0	1,10E-15	0
0,60396	0	0	0	0	0	0
0,61386	4,83E-09	0,5774	0	0	1,10E-15	0
0,62376	3,22E-09	0,7071	0	0	7,32E-16	0
0,63366	0	0	0	0	0	0
0,64356	1,61E-09	1	0	0	3,66E-16	0
0,65347	0	0	0	0	0	0
0,66337	1,61E-09	1	0	0	3,66E-16	0
0,67327	1,61E-09	1	0	0	3,66E-16	0
0,68317	0	0	0	0	0	0
0,69307	0	0	0	0	0	0
0,70297	1,61E-09	1	0	0	3,66E-16	0
0,71287	4,83E-09	0,5774	0	0	1,10E-15	0
0,72277	0	0	0	0	0	0
0,73267	1,61E-09	1	0	0	3,66E-16	0
0,74257	0	0	0	0	0	0
0,75248	3,22E-09	0,7071	0	0	7,32E-16	0
0,76238	3,22E-09	0,7071	0	0	7,32E-16	0
0,77228	0	0	0	0	0	0
0,78218	1,61E-09	1	0	0	3,66E-16	0
0,79208	4,83E-09	0,5774	0	0	1,10E-15	0
0,80198	1,61E-09	1	0	0	3,66E-16	0
0,81188	1,61E-09	1	0	0	3,66E-16	0
0,82178	1,61E-09	1	0	0	3,66E-16	0
0,83168	0	0	0	0	0	0
0,84158	0	0	0	0	0	0
0,85149	0	0	0	0	0	0
0,86139	1,61E-09	1	0	0	3,66E-16	0
0,87129	1,61E-09	1	0	0	3,66E-16	0
0,88119	0	0	0	0	0	0
0,89109	0	0	0	0	0	0
0,90099	0	0	0	0	0	0
0,91089	1,61E-09	1	0	0	3,66E-16	0
0,92079	1,61E-09	1	0	0	3,66E-16	0
0,93069	0	0	0	0	0	0
0,94059	0	0	0	0	0	0
0,9505	4,83E-09	0,5774	0	0	1,10E-15	0
0,9604	1,61E-09	1	0	0	3,66E-16	0
0,9703	0	0	0	0	0	0
0,9802	0	0	0	0	0	0
0,9901	0	0	0	0	0	0
1	0	0	0	0	0	0